Rock Mechanics and Rock Engineering (2022) 55:1445–1460
https://doi.org/10.1007/s00603-021-02749-9

ORIGINAL PAPER

Load Transfer Behavior During Cascading Pillar Failure: An Experimental Study

Hangyu Dong[1] · Wancheng Zhu[1] · Chen Hou[1] · Xige Liu[1]

Received: 26 January 2021 / Accepted: 12 December 2021 / Published online: 7 January 2022

Abstract

In order to reveal the load transfer mechanism during cascading pillar failure, compressive tests on treble-pillar specimens were conducted under soft and stiff loading conditions, where the stiffness of the test machine was adjusted with a disc spring group. Experimental results showed that the load transfer behavior of treble-pillar specimen could only be reproduced under soft loading condition when the rapid elastic rebound is achievable with disc spring group. The load transfer behavior of treble-pillar specimen is governed by energy storage characteristics of test machine and the mechanical properties of three rock specimens. In this respect, the failure behavior of treble-pillar specimen under soft loading condition was summarized into the following three failure modes: successive failure mode, compound failure mode and domino failure mode. Additionally, a theoretical model was proposed to further explain the physical mechanism of load transfer behavior, where the theoretical results of load transfer and elastic rebound of disc spring group were in good agreement with the experimental results. Finally, it was concluded that the elastic deformation of near-field surrounding rockmass (or the soft loading condition) was the necessary condition for load transfer of multiple pillars; and the rapid elastic rebound of near-field surrounding rockmass was the physical essence of load transfer behavior. This study may contribute to understanding the load transfer mechanism among pillars and to optimizing the design of room-and-pillar stopes during underground mining.

Highlights

- The soft loading condition of test machine is realized by adjusting the stiffness of disc spring group.
- The experiments on treble-pillar specimens are conducted to reveal the load transfer mechanism during cascading pillar failure.
- Three failure modes of treble-pillar specimen are successive failure, compound failure and domino failure.

Keywords Room-and-pillar mining · Cascading pillar failure · Treble-pillar specimen · Load transfer · Soft loading condition

List of symbols

c	Cohesion force
D_{T}	Total displacement of pillars-surrounding rockmass system
D_1, D_2	Displacement of near-field surrounding rockmass
d_{m}	Displacement of machine (or far-field surrounding rockmass)
d_{p}	Displacement of pillars
d_{s}	Deformation of disc spring group (or near-field surrounding rockmass)
d_1, d_2	Displacement of treble-pillar specimen
E	Elastic modulus of rock pillar specimen
F_1, F_2	Load at critical moment
i	Serial number of the undamaged pillar

✉ Wancheng Zhu
zhuwancheng@mail.neu.edu.cn

1 Department of Mining Engineering, Center for Rock Instability and Seismicity Research, School of Resource and Civil Engineering, Northeastern University, Shenyang 110819, China

K	Stiffness of near-field surrounding rockmass (or disc spring group)
k	Pre-peak stiffness of rock pillar specimen
k_i	Pre-peak stiffness of undamaged pillar i
k_{I}, k_{II}, k_{III}	Pre-peak stiffness of rock pillar specimen I, II and III
k_{p}	Post-peak stiffness of rock pillar specimen
k_{ud}	Pre-peak stiffness of undamaged intact pillar
N	Number of disk spring
n	Number of pillar
UCS	Uniaxial compression strength
ν	Poisson's ratio
σ_{t}	Tensile strength
φ	Internal friction angle
Δd	Sudden jump displacement of treble-pillar specimen (or elastic rebound of near field surrounding rockmass)
ΔF	Load drop of pillars-surrounding rockmass system
ΔF_i	Transferred load from damaged pillars to undamaged pillar i
ΔF_{I}, ΔF_{III}	Transferred load in Pillar I and Pillar III

1 Introduction

In the mining with room-and-pillar method, many pillars with different sizes and shapes were left behind as a temporary or permanent support, these pillars work with the surrounding rockmass to stabilize the underground stopes (Cording et al. 2015; Xia et al. 2019; Zhang et al. 2017). However, with the increase of mining depth, the unstable pillar failure has been widespread in underground mines and seriously threatens the safety of workers and equipment (Dehghan et al. 2013; Esterhuizen et al. 2019; Peng 2007; Szwedzicki 2001; Zipf 2011). Swanson and Boler (1995) coined the term "cascading pillar failure" to describe the collapses of pillars. Cascading pillar failure in room-and-pillar mines can also be termed as "progressive pillar failure", "massive roof collapse", "domino-type failure", or "pillar run" (Zipf 2011).

During underground mining, pillars may fail in different manner, depending on the mechanical behavior of pillars and mining layout. In some cases, only a few tens of pillars fail; however, in extreme cases, hundreds, even thousands of pillars can fail. On January 21, 1960, a massive pillar collapse in the Coalbrook Coal Mine in South Africa killed 437 people and created a 2,000,000 m^2 subsidence area (Szwedzicki 2001). A remaining pillar failure in Fetr6 Chromite Mine led to a progressive failure of pillars within 4000 m^2 in a few minutes (Dehghan et al. 2013). The sudden collapse of approximately 35 pillars involving 30,000 m^2 underground areas at a limestone mine in southwestern Pennsylvania resulted in an air blast that injured three mine workers in 2015 (Esterhuizen et al. 2019). The pillar collapse occurred in the Lewiston–Stockton Coal Seam in 1986, causing a collapse area with a radius of 100 m, and a roof subsidence of 0.5 m (Peng 2007). The cascading pillar failure in China Xingtai gypsum mine induced a subsidence area with along axis of 300 m and short axis of 210 m (Wang et al. 2008). The total area of collapsed land on surface reaches 53,000 m^2, and the maximum subsidence in the central area of the collapsed surface is about 8.0 m. It was also reported that US coal and non-metal mines had at least eight and five of these kinds of pillar failures, respectively, in the 1990s (Zipf 2011).

Many efforts have been devoted to study the failure mechanism of pillars, which is closely related to the transferred load from collapsing pillars to adjacent pillars (Zhou et al. 2018a, 2019, 2020; Zhu et al. 2018, 2020). In other words, the failure of one critical pillar could possibly trigger the collapse of a large areas of the mine when transferred load exceeds the bearing capacities of adjacent pillars (Cording et al. 2015; Zhou et al. 2017; Zipf 1996; Zipf and Mark 1997). Zhou et al. (2017) gave experimental and numerical results on the failure process of double-pillar specimen, and found that the pillar with higher elastic modulus or lower strength would lose its bearing capacity firstly. In this respect, an individual pillar with higher elastic modulus or lower strength was the weak link of a group of pillars. Zhou et al. (2018b) also studied the collapse of mined-out areas triggered by residual pillar extraction, and they considered that the magnitude of the dynamic disturbance to adjacent pillars was closely related to extraction time of the residual pillar. Moreover, the load transfer and collapse of pillars were not only related to the mechanical properties of the pillar itself, but also greatly affected by the stiffness of the surrounding rockmass (Chen et al. 1997; Gao et al. 2019; Kaiser and Tang 1998; Wang et al. 2011). Wang et al. (2011) carried out numerical analysis on the failure mechanism of multi-pillar system and revealed that the stiffness and uniaxial compressive strength (UCS) of pillar played important roles in controlling the failure process of multi-pillar system. Kaiser and Tang (1998) studied the effect of elastic rebound of roof and floor on the failure mode of single pillar specimen by using RFPA^{2D} and confirm that soft loading system promotes unstable failure or collapse of pillars. These studies have given us good understanding of the failure behavior of multi-pillar system.

However, the physical essence of cascading pillar failure lies in the interaction among these pillars and the associated load transfer mechanism among pillars is still unclear. Moreover, the existing experiments were not effective in quantifying the elastic energy storage and release in roof (or surrounding rockmass). Thus, the mechanism associated

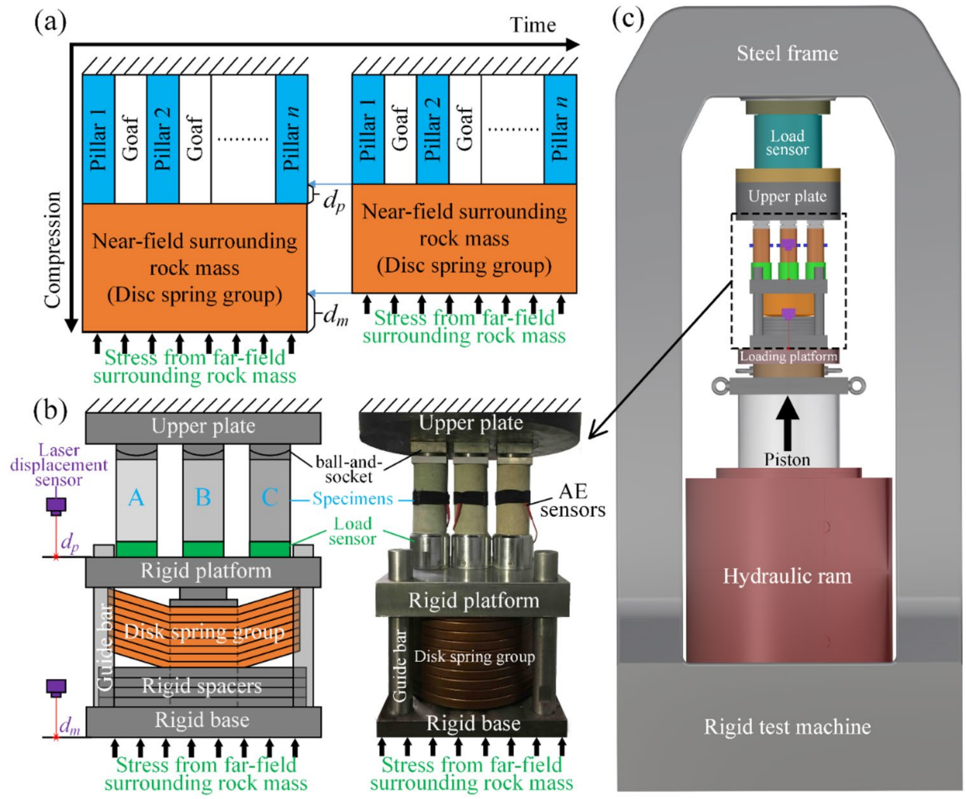

Fig. 1 Schematic diagram of physical model and experimental method. **a** Physical model of pillars-surrounding rockmass system, **b** experimental method of cascading pillar failure, **c** schematic diagram of experimental setup

with the load transfer behavior during the cascading pillar failure and accompanying elastic rebound of surrounding rockmass should be clarified further in order to understand the instability mechanism of cascading pillar failure during underground mining.

In this study, first, the experimental scheme of unstable failure of treble-pillar specimen was designed based on the cascading pillar failure in room and pillar mining. Then, the uniaxial compressive tests on treble-pillar specimens were conducted in order to study the load transfer behavior during the cascading pillar failure. Finally, a theoretical model was proposed to further quantify the load transfer mechanism during the cascading pillar failure.

2 Experimental Schemes

A physical model composed of pillars and surrounding rockmass is proposed, as shown in Fig. 1a. The system consisted of parallel pillars and near-field surrounding rockmass, where the stress from the far-field surrounding rockmass is applied as a boundary condition. The near-field surrounding rockmass is in elastic stage during the experiments, and it can store a large amount of elastic deformation energy under compression, which may have a major effect on the load transfer and instability of pillars (Gao et al. 2019; Ma et al. 2018).

The experimental apparatus as shown in Fig. 1b, c are designed. By comparing Fig. 1a with Fig. 1b, the far-field surrounding rockmass is represented as the stress boundary condition with a constant loading rate through the movement of piston of rigid test machine (displacement-control model with loading rate of 0.003 mm/s); while the near-field surrounding rockmass is denoted as the disk spring group, which may deform elastically with designed stiffness (K) and realize the soft loading condition with adjustable stiffness. The treble-pillar specimen (A, B and C) is used to simulate the parallel pillars. Figure 1c shows the rigid servo-control test machine, with a maximum axial load of 300 T. The displacement measurement range is 0–100 mm, the minimum loading rate is 0.001 mm/s and the steel frame stiffness is about 5 GN/m.

In this respect, the disc spring group can simulate the elastic deformation and energy storage of near-field surrounding rockmass. The stiffness of disc spring group (K) can be adjusted by changing the number (N) of disc spring. The load–displacement curve of disc spring group composed of ten disk springs is shown in Fig. 2. During experiments, the disc spring group will be at linear elastic stage when compressive displacement exceeds 0.5–1 mm because of the small gaps between disc springs, which has little effect on the deformation and failure behavior of treble-pillar specimen. The disc spring group is in elastic state during the

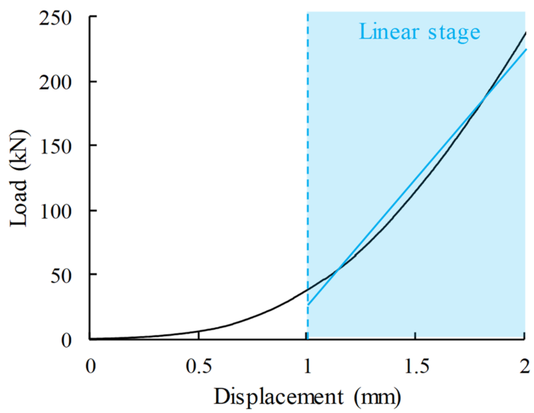

Fig. 2 Load–displacement curves of disc spring group with ten disk springs

whole compressive tests of treble-pillar specimens without permanent deformation.

Before the installation of treble-pillar specimen, the disc spring with specific stiffness was assembled and placed on the loading platform of testing machine. After the installation of treble-pillar specimen, uniaxial load was applied with displacement-control model (0.003 mm/s). Three load sensors were used to monitor the load of each pillar specimen (A, B and C); and three ball-and-socket devices were used to adjust the load from test machine so that each pillar specimen was under uniaxial compression. Two laser displacement sensors were used to measure the displacement of treble-pillar specimen (d_p) and the displacement of the test machine (d_m), respectively. The rock failure instability is closely governed by the loading stiffness of test machine. In this regard, the test machine used in this study is rigid enough to meet the stiff loading condition of this rock specimen, and the soft loading condition is achieved by padding disc spring group with adjustable stiffness between the specimens and loading plate in order to quantify the stiffness of test machine. In order to obtain the whole load–displacement curve of the specimen, the high-frequency laser displacement sensor and load sensor are connected to the high-speed data-acquisition instrument (sampling frequency 2 kHz), and then the complete displacement and load data of specimen can be obtained to draw the whole load–displacement curve of rock specimens. The difference (d_s) between d_p and d_m is the elastic deformation of the disk spring group. The failure of the treble-pillar specimen was monitored with the acoustic emission (AE) equipment of Physical Acoustics Corporation (PAC). Each pillar specimen was pasted with two AE sensors. The AE sensor (NANO-30) with frequency range of 125–750 kHz was used in the experiment, which could cover the frequency range of pillar specimen (mainly distributed in 150–260 kHz). And the sampling frequency of AE equipment was set as 3 MHz to collect the AE data when pillar collapses according to the Shannon sampling theorem (Shannon 1948). The pre-amplification was set as 40 dB; and AE signals whose amplitude exceeds 40 dB were collected.

During the uniaxial compressive test, the following should be emphasized that: (1) the total stiffness of loading system in Fig. 1b (including ball-and-socket, load sensor, rigid platform, spacer and base, but excluding disc spring group) is 3.919 GN/m, which is greater than the absolute value of post-peak stiffness of the treble-pillar specimen (1.982 GN/m). Therefore, according to the stiffness criterion (Salamon 1970), the instability of treble-pillar specimen is mainly affected by the stiffness of disc spring group. (2) The heights of each pillar specimen are same to ensure that they are subjected to force at the same displacement. We measured that there was very small deflection (about 0.03 mm) at the upper plate and rigid platform of the test machine when one of the pillars failed unstably, this deflection was much smaller than the sudden jump displacement of treble-pillar specimen when any pillar specimen occur instability, so its effect could be ignored.

As shown in Table 1, five kinds of sandstone specimens with different mechanical properties are tested, where the elastic modulus and strength of sandstone specimens have wide range. Letters G, W, Y, FY** and R represent green, white, yellow, fine yellow and red sandstone, respectively. The sandstone specimens were retrieved from Zigong City, Sichuan, China, with good homogeneity. The size of the specimens is $\phi 50$ mm $\times$ 100 mm. The elastic modulus (E), uniaxial compression strength (UCS), cohesion force (c), tensile strength (σ_t), internal friction angle (φ), Poisson's

Table 1 Basic mechanical parameters of sandstone specimens

Rock type	E (GPa)	UCS (MPa)	σ_t (MPa)	c (MPa)	φ (°)	ν	k (kN/mm)	k_p (kN/mm)
Green sandstone (G)	10.03	78.84	8.07	12.57	41.47	–	196.88	1178.67
White sandstone (W)	5.75	49.06	4.85	8.44	45.18	0.186	112.81	843.01
Yellow sandstone (Y)	2.52	43.65	2.78	10.56	38.56	0.173	49.45	532.11
Fine yellow sandstone (FY)	4.89	48.20	3.60	8.9	36.2	0.256	96.05	671.03
Red sandstone (R)	3.27	24.85	1.62	3.27	54.3	0.215	64.16	332.25

Table 2 Experimental schemes to reproduce cascading pillar failure with different combination mode

Combination Mode	Items	Soft loading condition	Stiff loading condition
W–Y–R	Schematic diagram	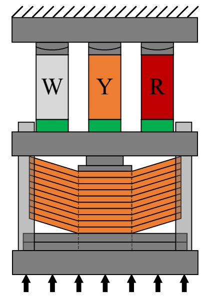	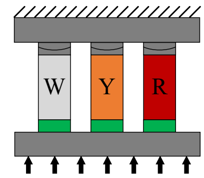
	Number of disc spring	10	None
Y–R–Y	Schematic diagram	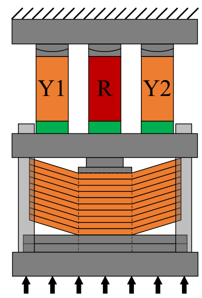	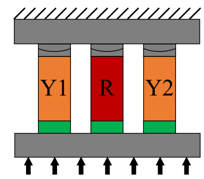
	Number of disc spring	10	None
G–FY–Y	Schematic diagram	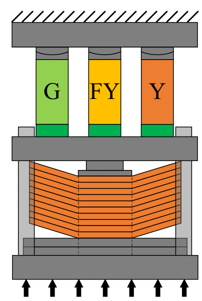	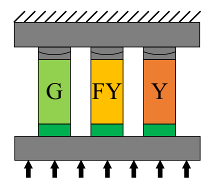
	Number of disc spring	10	None

ratio (ν), pre-peak stiffness (k) and post-peak stiffness (k_p) of different sandstone specimens are listed in Table 1.

The experimental schemes listed in Table 2 are used to quantify the cascading pillar failure and load transfer behavior of treble-pillar specimen by combining the five kinds of sandstone specimens. Treble-pillar specimens, named as W–Y–R, Y–R–Y and G–FY–Y specimens in Table 2, are tested under soft loading condition using disc spring group and under stiff loading condition without using disc spring group, respectively.

Additionally, according to Labuz and Biolzi (1991) and Chen et al. (2008), the shorter the rock specimen, the more likely for stable softening to occur in the uniaxial compression of one rock specimen. And the more parallel pillars in the system, the more energy dissipation is associated within the post-peak stage, which means that the post-peak stage is much smoother and less prone to instability. Thus, the size and number of parallel pillars should be considered in our future study.

3 Experimental Results

3.1 W–Y–R Specimen

Figure 3 shows the experimental results of W–Y–R specimen under soft loading condition. Pillar R, Pillar W and Pillar Y fail in order at 828.02, 898.52 and 942.10 s, respectively. (1) Pillar R fails first with a load drop (66.44 kN), resulting in the sudden increases of load (which is called the load transfer) in Pillar W (17.52 kN) and Pillar Y (10.77 kN), as shown in Fig. 3a. The failure of Pillar R causes the elastic rebound (0.18 mm) and elastic energy release (3.61 J) of disc spring group; and the elastic energies of Pillar W and Pillar Y respectively increases by 1.75 and 0.66 J due to the elastic rebound of disc spring group, as shown in Fig. 3b, c. Therefore, the elastic energy transfer ratio from disc spring group to treble-pillar specimen is defined as: (1.75 J + 0.66 J)/3.61 J ≈ 66.76%. (2) Pillar W fails subsequently with a load drop (104.26 kN), resulting in the

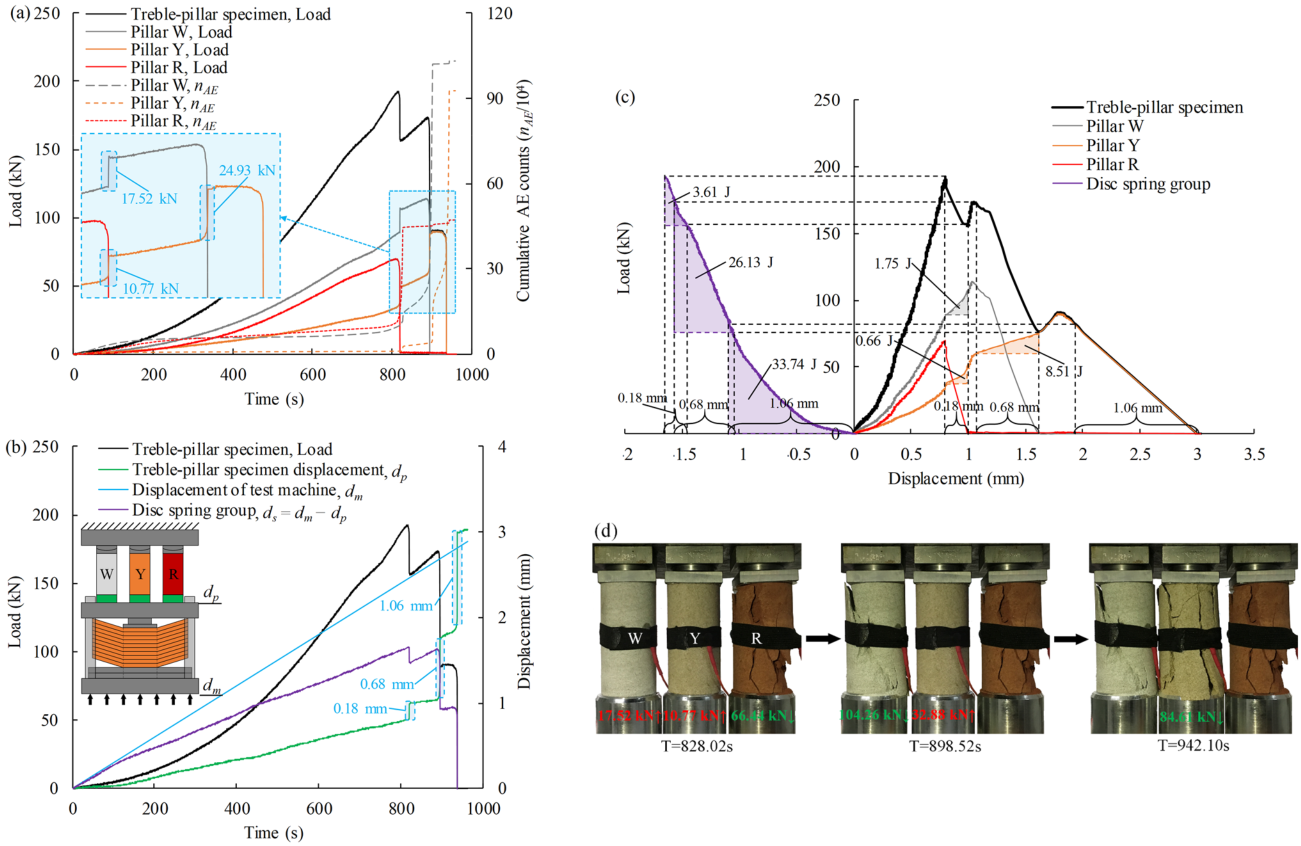

Fig. 3 Experimental results of W–Y–R specimen under soft loading condition. **a** Load and cumulative AE counts versus time; **b** load and displacement versus time; **c** load–displacement curves of pillars and disc spring group; **d** failure patterns

sudden increase of load (or load transfer) in Pillar Y (24.93 kN), as shown in Fig. 3a. The failure of Pillar W causes the elastic rebound (0.68 mm) and elastic energy release (26.13 J) of disc spring group; and the elastic energy of Pillar Y increases by 8.51 J due to the elastic rebound of disc spring group, as shown in Fig. 3b, c. Therefore, the elastic energy transfer ratio from disc spring group to treble-pillar specimen is calculated as: 8.51 J/26.13 J ≈ 32.57%. (3) Pillar Y fails finally with a load drop (84.61 kN), causing the elastic rebound (1.06 mm) and elastic energy release (33.74 J) of disc spring group, as shown in Fig. 3a–c.

The elastic energy was calculated by the formula $E = 0.5k\Delta d^2$. E refers to elastic energy release of disc spring group or the elastic energy increase of pillar specimen; k refers to the stiffness of disc spring group or pillar specimen; and Δd refers to the sudden jump displacement (elastic rebound) of disc spring group and pillar specimen.

As a comparison, W–Y–R specimen under stiff loading condition fail in order at 326.73, 432.49 and 495.81 s, respectively, with load drops (58.61, 122.86 and 70.85 kN), as shown in Fig. 4. However, the failure of single pillar in W–Y–R specimen under stiff loading condition does not cause the sudden increases of load (or load transfer) and elastic energy in adjacent pillars due to the lack of elastic rebound of disc spring group, as shown in Fig. 4a–c. The experimental duration under soft loading condition is approximately twice the length than that under stiff loading condition due to the buffering and energy absorbing of disc spring group (e.g. 942.10 s under soft loading condition and 495.81 s under stiff loading condition).

From Fig. 3a, it is observed that the failure of single pillar in W–Y–R specimen under soft loading condition not only induces the sudden increase of cumulative AE counts in itself, but also leads to the sudden increases in adjacent pillars by load transfer. For example, Pillar Y experienced three sudden increases of cumulative AE counts. The first sudden increase was related to the failure of Pillar R; the second sudden increase was related to the failure of Pillar W; and the third sudden increase indicated the failure of Pillar Y itself. However, as shown in Fig. 4a, the failure of single pillar in W–Y–R specimen under stiff loading condition only causes the sudden increase of cumulative AE counts in itself but has no effect on adjacent pillars, because there is no load transfer in adjacent pillars due to the lack of elastic rebound of disc spring group.

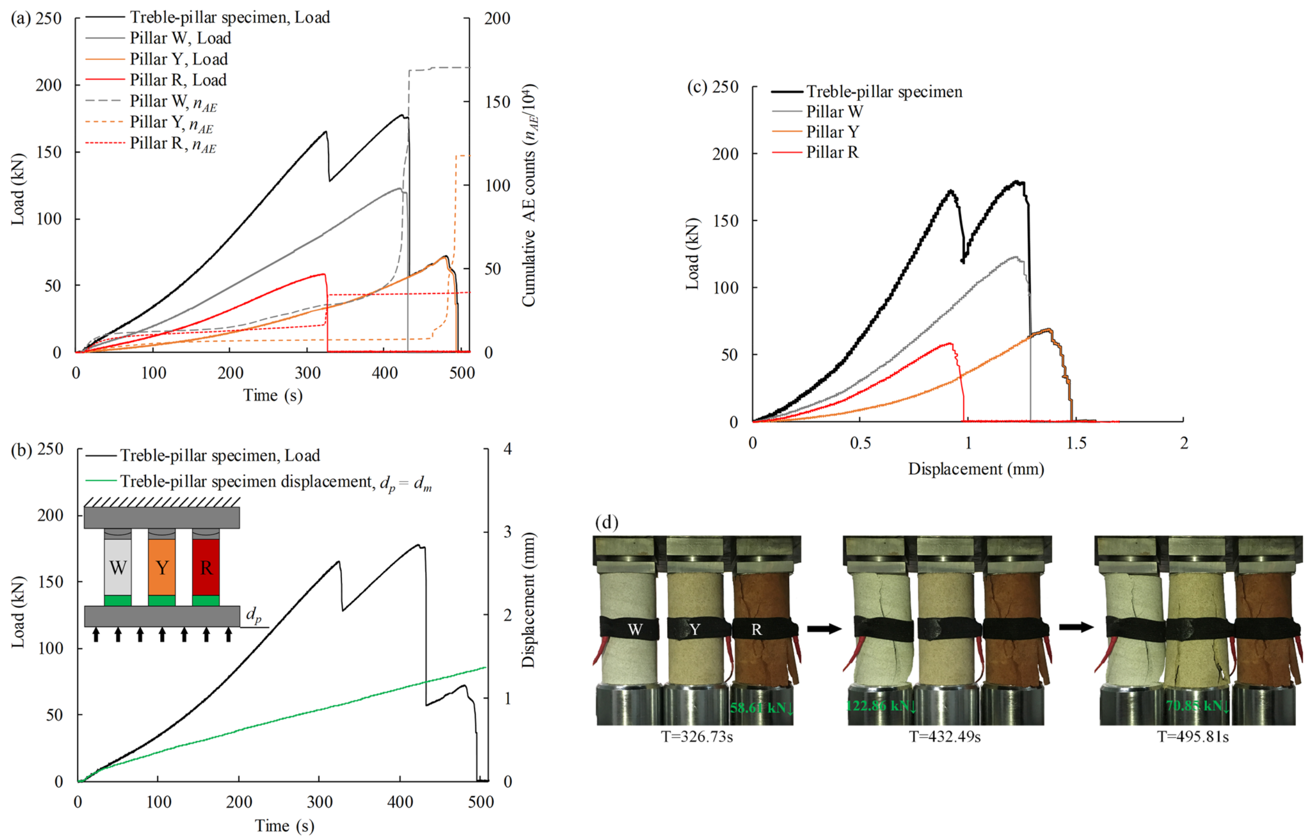

Fig. 4 Experimental results of W–Y–R specimen under stiff loading condition. **a** Load and cumulative AE counts versus time; **b** load and displacement versus time; **c** load–displacement curves of pillars and disc spring group; **d** failure patterns

Figure 3d shows the failure patterns of W–Y–R specimen under soft loading condition, where Pillar R, Pillar W and Pillar Y fails abruptly at 828.02, 898.52 and 942.10 s with loud noise due to the violent elastic rebound of disc spring group. Rock debris ejects from the lower right corner of Pillar R. A shear band forms at an orientation of 60°–65° from the top left corner to the lower right corner in Pillar W. Multiple splitting fractures form along the axial direction in Pillar Y. By comparing Fig. 3d with Fig. 4d, the failure patterns of W–Y–R specimen under soft loading condition is generally more fragmented than that under stiff loading condition due to the violent elastic energy release of disc spring group.

3.2 Y–R–Y Specimen

As for the treble-pillar specimen (Y–R–Y specimen) under soft loading condition, (1) Pillar R fails first at 899.08 s with a load drop (28.45 kN), resulting in the sudden increases of load (or load transfer) in Pillar Y1 (6.26 kN) and Pillar Y2 (6.92 kN), as shown in Fig. 5a. The failure of Pillar R causes the elastic rebound (0.07 mm) and elastic energy release (0.85 J) of disc spring group, and the elastic energies of Pillar Y1 and Pillar Y2, respectively, increase by 0.119 and 0.121 J due to the elastic rebound of disc spring group, as shown in Fig. 5b, c. Therefore, the elastic energy transfer ratio from disc spring group to treble-pillar specimen is calculated as follows: (0.119 J + 0.121 J)/0.85 J ≈ 28.24%. (2) And then Pillar Y1 and Pillar Y2 fail simultaneously at 1196.38 s with load drops (99.88 and 86.11 kN), as shown in Fig. 5a. By amplifying the failure process of pillars Y1 and Y2 shown in Fig. 5a, the load transfer behavior between Y1 and Y2 (which is smaller than 200 ms) is clearly observed: the failure of Y2 induces the sudden increase of load (or load transfer) in Y1 (10.91 kN), which exceeds the bearing capacity of Y1 and causes its failure. The simultaneous failure of Pillar Y1 and Pillar Y2 causes the elastic rebound (1.71 mm) and elastic energy release (107.25 J) of disc spring group; and the elastic rebound of disc spring group causes the sudden increase of elastic energy in Pillar Y1 (0.82 J), as shown in Fig. 5b, c. Therefore, the elastic energy transfer ratio from disc spring group to treble-pillar specimen is calculated as: 0.82 J/107.25 J ≈ 0.76%.

Different from soft loading condition, Pillar R, Pillar Y1 and Pillar Y2 of Y–R–Y specimen under stiff loading condition fail separately at 371.81, 575.23 and 604.89 s with

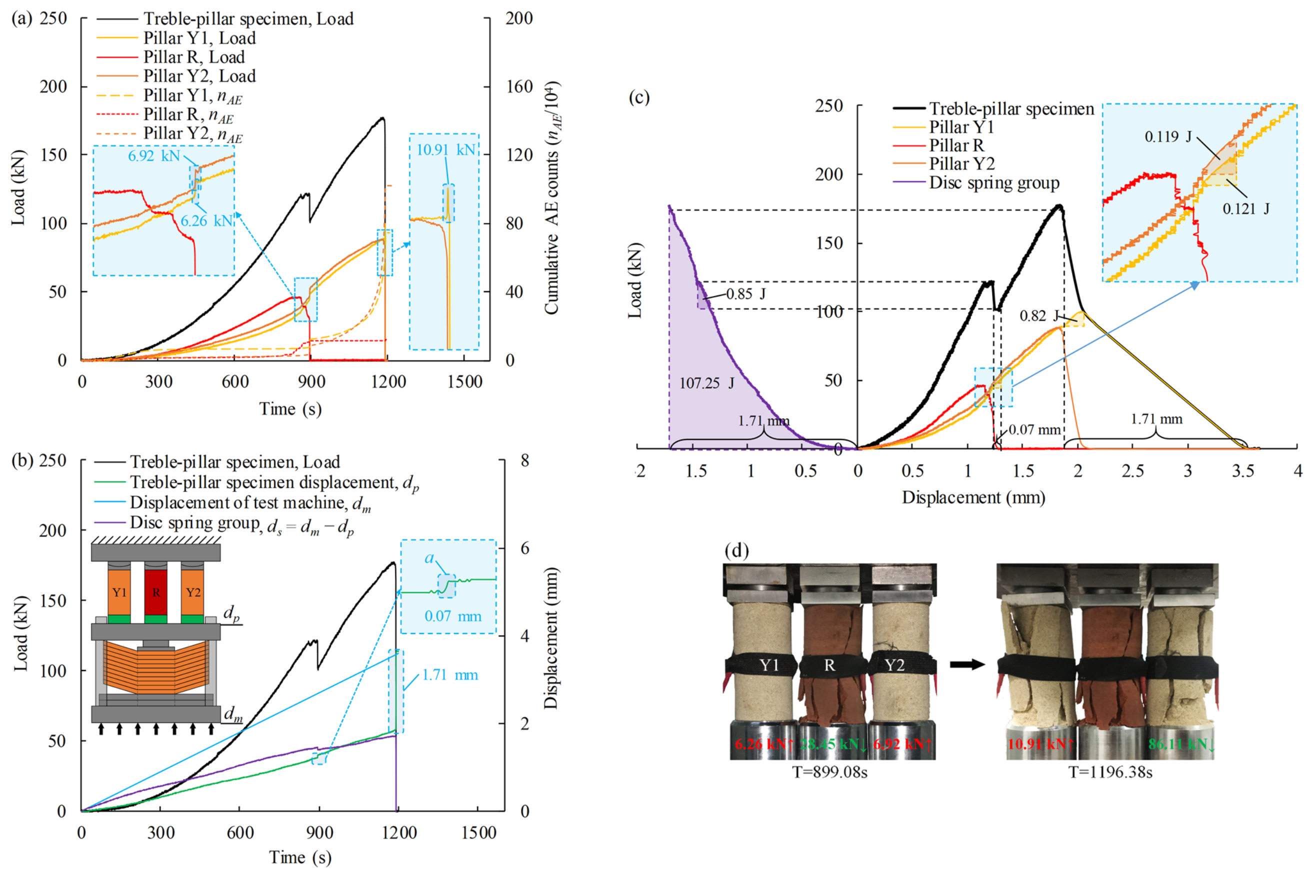

Fig. 5 Experimental results of Y–R–Y specimen under soft loading condition. **a** Load and cumulative AE counts versus time; **b** load and displacement versus time; **c** load–displacement curves of pillars and disc spring group; **d** failure patterns

load drops (56.37, 95.41 and 90.54 kN), as shown in Fig. 6a. And the failure of single pillar does not cause the sudden increase of load (or load transfer) and elastic energy in adjacent pillars due to the lack of disc spring group, as shown in Fig. 6a–c. The experimental duration of Y–R–Y specimen under soft loading condition is approximately twice the length than that under stiff loading condition due to the buffering and energy absorbing of disc spring group (e.g. 1196.38 s under soft loading condition and 604.89 s under stiff loading condition).

From Fig. 5a, it is observed that the failure of Pillar R in Y–R–Y specimen under soft loading condition not only induces the sudden increase of cumulative AE counts in itself, but also leads to the sudden increases in adjacent pillars Y1 and Y2 by load transfer. However, as shown in Fig. 6a, the failure of Pillar R in Y–R–Y specimen under stiff loading condition only causes the increase of cumulative AE counts in itself but has no effect on adjacent pillars Y1 and Y2 because there is no load transfer in adjacent pillars.

As shown in Fig. 5d, Pillar Y1 and Pillar Y2 of Y–R–Y specimen under soft loading condition fail simultaneously at 1196.38 s due to the load transfer; while Pillar Y1 and Pillar Y2 of Y–R–Y specimen under stiff loading condition fail separately at 575.23 and 604.89 s, respectively, as shown in Fig. 6d. By comparing Fig. 5d with Fig. 6d, the failure patterns of Y–R–Y specimen under soft loading condition are observed to be much more violent than that under stiff loading condition due to the violent elastic rebound of disc spring group. For example, Pillar R under soft loading condition ejects more debris than that under stiff loading condition; and the failure patterns of Y1 and Y2 under soft loading condition are more fragmented than that under stiff loading condition.

3.3 G–FY–Y Specimen

Figure 7 shows the experimental results of G–FY–Y specimen under soft loading condition, where all pillars fall abruptly and simultaneously within a very short time (120 ms). Pillar G, Pillar FY and Pillar Y fail simultaneously at 1086.36 s with load drops (144.57, 132.39 and 118.81 kN), as shown in Fig. 7a. By amplifying the failure process

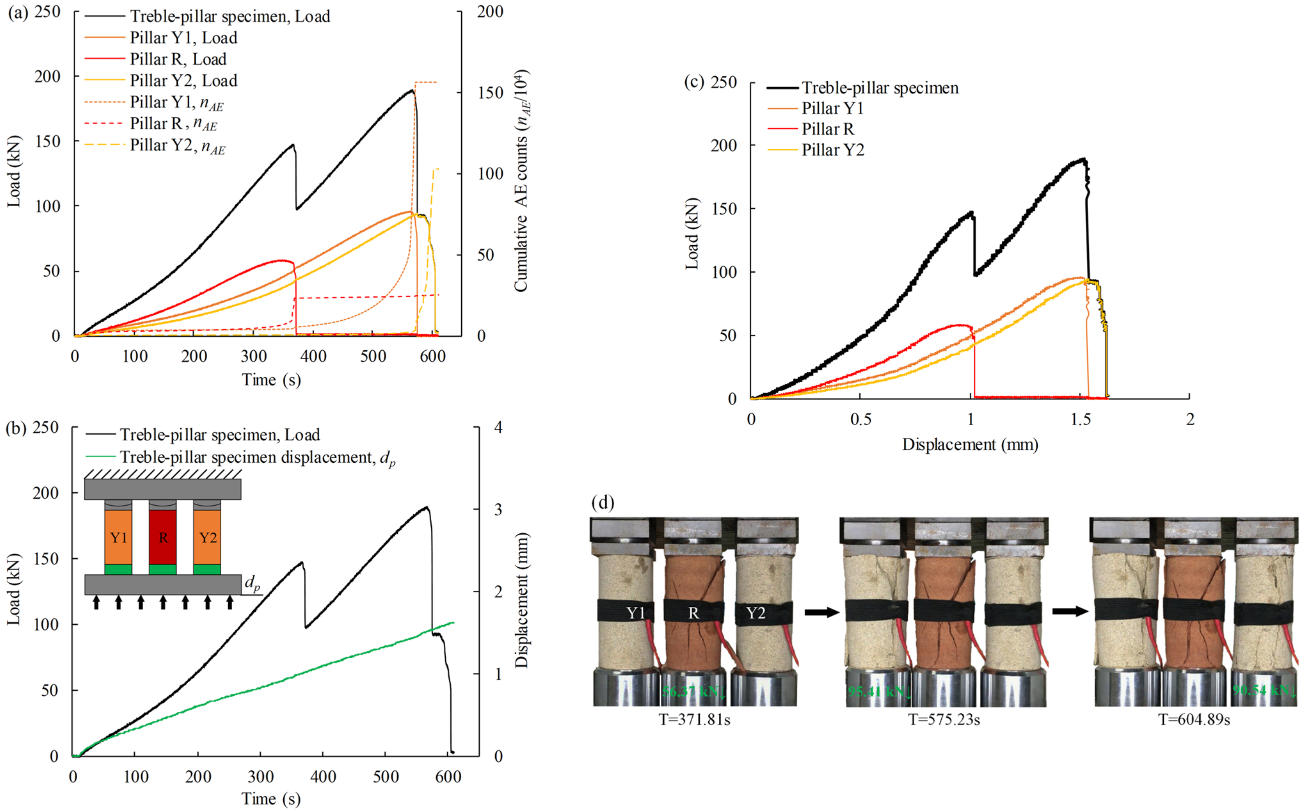

Fig. 6 Experimental results of Y–R–Y specimen under stiff loading condition. **a** Load and cumulative AE counts versus time; **b** load and displacement versus time; **c** load–displacement curves of pillars and disc spring group; **d** failure patterns

of pillars G, FY and Y shown in Fig. 7a, the load transfer behavior among them is clearly observed: the failure of Pillar G induces the sudden increase of load (or load transfer) in FY (38.77 kN) and Y (35.21 kN), which exceeds the bearing capacities of pillars FY and Y and causes their failures. The simultaneous failure of Pillar G, Pillar FY and Pillar Y causes the total elastic rebound (1.55 mm) and elastic energy release (159.24 J) of disc spring group; and the elastic rebound of disc spring group causes the sudden increases of elastic energy in Pillar FY (5.02 J) and Pillar Y (8.17 J), as shown in Fig. 7b, c. Therefore, the elastic energy transfer ratio from disc spring group to treble-pillar specimen is calculated as follows: (5.02 J + 8.17 J)/159.24 J ≈ 8.28%.

Different from G–FY–Y specimen under soft loading condition, Pillar G, Pillar FY and Pillar Y of G–FY–Y specimens under stiff loading condition fail separately at 475.47, 517.92 and 560.19 s with load drops (163.43, 51.61 and 66.89 kN), as shown in Fig. 8a. And the failure of single pillar does not cause the sudden increase of load (or load transfer) and elastic energy in adjacent pillars due to the lack of disc spring group, as shown in Fig. 8a–c. The experimental duration of G–FY–Y specimen under soft loading condition is approximately twice the length than that under stiff loading condition due to the buffering and energy absorbing of disc spring group (e.g. 1086.36 s under soft loading condition and 560.20 s under stiff loading condition).

Figure 7d shows the failure patterns of G–FY–Y specimen under soft loading condition. Rock blocks were ejected and scattered on the platform with a loud sound, and the pillars were seriously damaged by the elastic energy release. By comparing Fig. 7d with Fig. 8d, the failure patterns under soft loading condition were seen to be more violent than that under stiff loading condition due to the violent elastic rebound of disc spring group.

It should be noted that the instability process of G–FY–Y specimen under soft loading condition is spontaneously completed without continued external loading from test machine. The instability is driven by the load transfer due to the elastic rebound of disc spring group. In this regard, the near-field surrounding rockmass (simulated with disc spring group) has played an important role in the load transfer and instability of pillars.

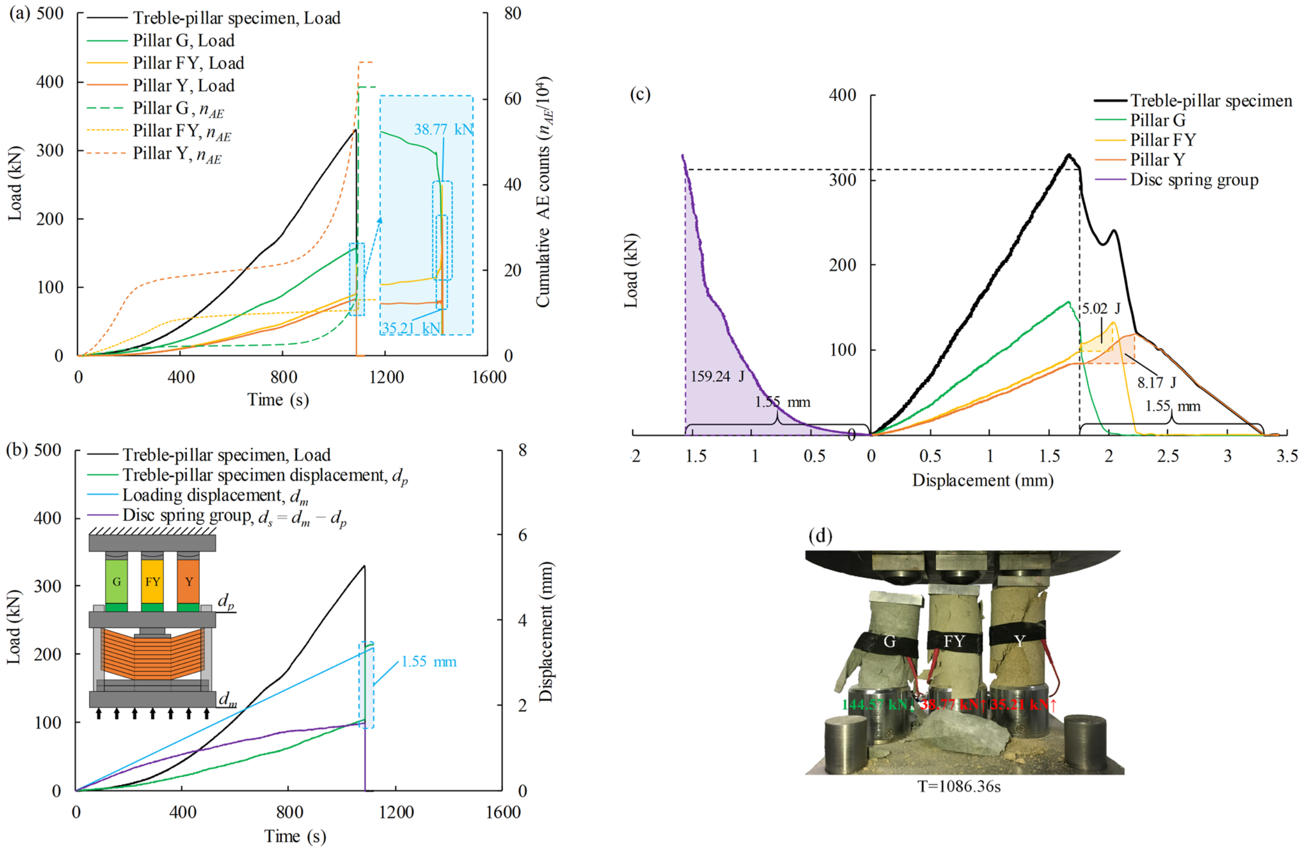

Fig. 7 Experimental results of G–FY–Y specimen under soft loading condition. **a** Load and cumulative AE counts versus time; **b** load and displacement versus time; **c** load–displacement curves of pillars and disc spring group; **d** failure patterns

4 Analysis of Results

4.1 Failure Process

According to the experimental results in Sect. 3, it is concluded that the elastic deformation of near-field surrounding rockmass (or the soft loading condition) is the necessary condition for the load transfer among the multiple pillars; and the rapid elastic rebound of near-field surrounding rockmass is the physical essence that induces the load transfer behavior. In addition, the failure behavior of different combinational modes can be summarized into three typical failure modes, which are *successive failure mode*, *compound failure* mode and *domino failure mode*:

(1) Figure 9a summarizes the failure behavior of W–Y–R specimen into *successive failure mode*. When Pillar R fails first in Stage 2, the near-field surrounding rockmass will rebound and compress the remaining pillars, resulting in the load and elastic energy transfers (or increases) in Pillar W and Pillar Y. As the load transfer does not exceed the bearing capacity of Pillar W or Pillar Y, continued loading from far-field surrounding rockmass in Stage 3 is needed to complete the failure of remaining pillars. Then, Pillar W fails second in Stage 4 with elastic rebound of near-field surrounding rockmass, causing the load and elastic energy transfer (or increases) in Pillar Y. Similarly, the load transfer does not exceed the bearing capacity of Pillar Y. Finally, Pillar Y fails with an elastic rebound of near-field surrounding rockmass under the continued loading of far-field surrounding rockmass from Stage 5 to Stage 6.

In summary, the *successive failure mode* requires the continued loading from far-field surrounding rockmass to complete the destruction of all pillars one by one because the load transfer magnitude caused by one pillar's collapse does not exceed the bearing capacity of adjacent pillars. In addition, the elastic energy transfer ratio from disc spring group to treble-pillar specimen experiences a decrease from 66.76 to 32.57% because the elastic rebound of near-field surrounding rockmass will increase with the decrease of the number of pillars. And the elastic rebound of near-field surrounding rockmass experiences an increase from 0.18 mm to 1.06 mm, which means more elastic energy release of disc spring group.

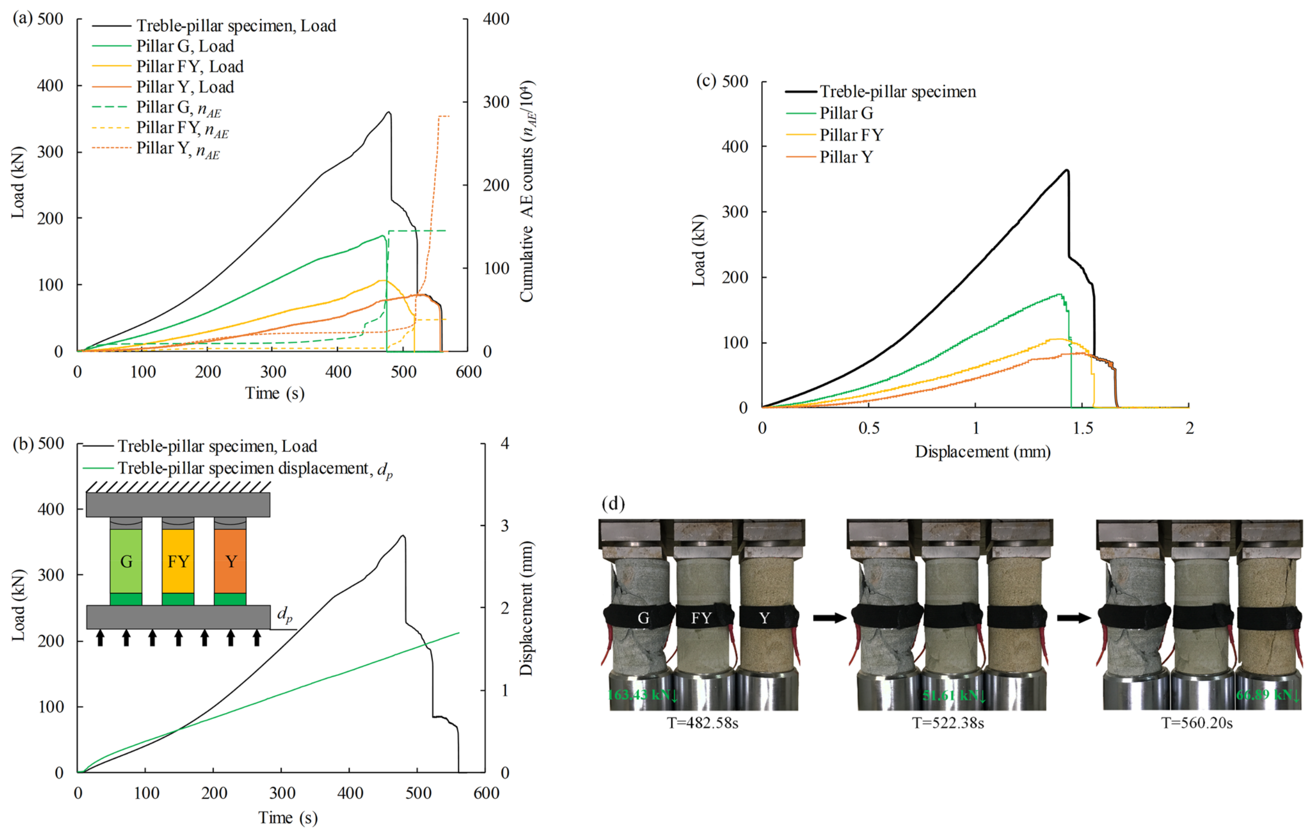

Fig. 8 Experimental results of G–FY–Y specimen under stiff loading condition. **a** Load and cumulative AE counts versus time; **b** load and displacement versus time; **c** load–displacement curves of pillars and disc spring group; **d** failure patterns

(2) Figure 9b defines the failure behavior of Y–R–Y specimen as *compound failure mode*. When Pillar R fails first in Stage 2, the near-field surrounding rockmass will rebound and compress the remaining pillars, resulting in the load and elastic energy transfers (or increases) in Pillar Y1 and Pillar Y2. The load transfer does not exceed the bearing capacity of pillars Y1 and Y2. However, with the continued loading of far-field surrounding rockmass in Stage 3, pillars Y1 and Y2 fail simultaneously at Stage 4 because the load transfer exceeds the bearing capacity of Pillar Y1.

(3) Figure 9c summarizes the failure behavior of G–FY–Y specimen into *domino failure mode*. With the continued loading of far-field surrounding rockmass in Stage 1, pillars G, FY and Y fail simultaneously at Stage 2. The load transfer induced by the failure of Pillar G exceeds the bearing capacity of pillars FY and Y, which causes the simultaneous failure of treble-pillar specimen. The instability process of pillars is spontaneously completed without the continued external loading from far-field surrounding rockmass; and the whole instability process was driven by the elastic rebound of near-field surrounding rockmass. Thus, the *compound failure mode* is a transition mode between the *successive failure mode* and the *domino failure mode*, which includes the failure behavior caused by continued external loading and load transfer. In addition, the *domino failure mode* has a low energy transfer ratio (8.28%), because the *domino failure mode* releases all elastic energy at one time, while the *successive failure mode* and *compound failure mode* release the elastic energy gradually more than one time.

4.2 Theoretical Analysis

The failure of one pillar will result in the load drop of pillars-surrounding rockmass system (Vardar et al. 2017). In this respect, when one pillar fails abruptly, the near-field surrounding rockmass will undergo rapid elastic rebound due to the decrease of far-field load; Meanwhile, the remaining pillars will undergo the same amount of compressed displacement, which causes the increases of load (the load transfers) to the adjacent pillars. When the load transfers exceed the bearing capacity of adjacent pillars, the failures will occur; and then the load transfer will continue and may lead to more pillars collapse; thus the cascading pillar failure occurs.

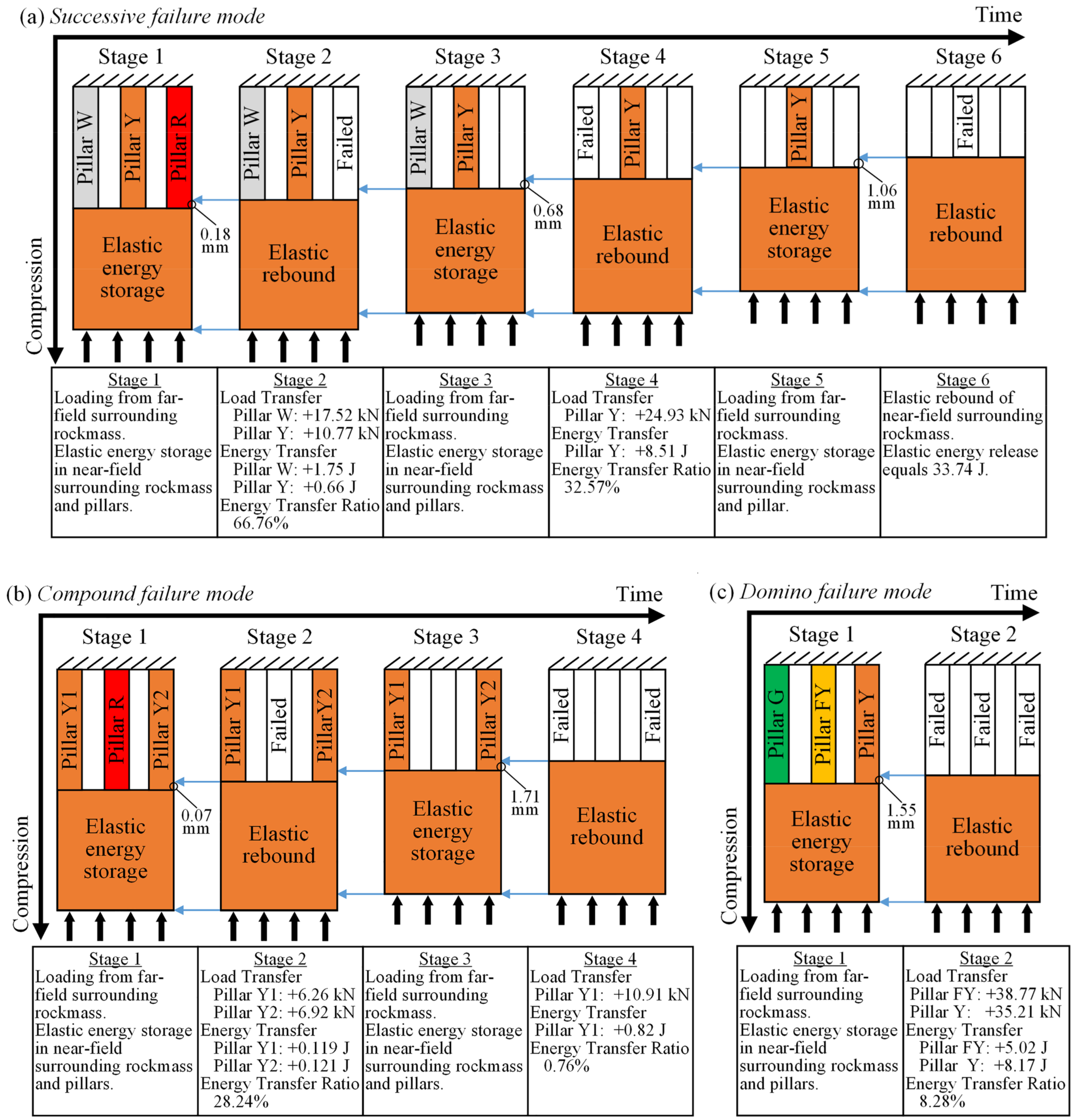

Fig. 9 Schematic diagram of instability and load transfer behavior of treble-pillar specimen of three pillar Failure modes. **a** Successive failure mode; **b** Compound failure mode; **c** Domino failure mode

In order to verify the hypothesis, we gave theoretical analysis on the failure process of treble-pillar specimen under soft or stiff loading conditions. Under the soft loading condition, the elastic deformation and rebound of near-field surrounding rockmass was considered; while under stiff loading condition, the surrounding rockmass is regarded as rigid body without elastic rebound. As shown in Fig. 10, a treble-pillar specimen is loaded quasi-statically under soft or stiff loading condition. Thus, pillars I, II and III will have same vertical displacement increments during the compression. The pre-peak stiffness of pillars I, II and III are k_{I}, k_{II} and k_{III}, respectively. And the stiffness of near-field surrounding rockmass (or disc spring group) is K.

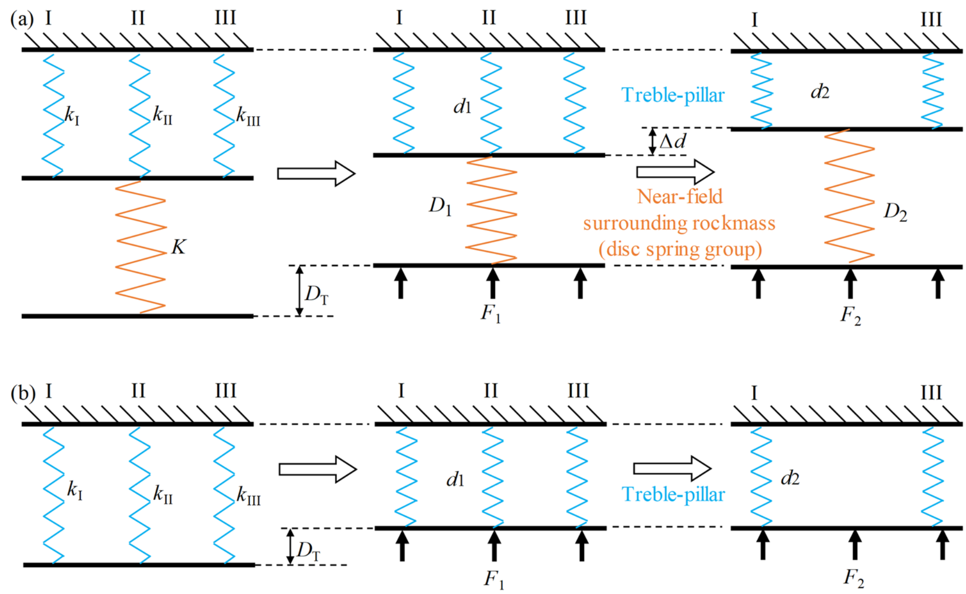

Fig. 10 Simplified mechanical model of treble-pillar specimen under different loading condition. **a** Soft loading condition; **b** stiff loading condition

As shown in Fig. 10a, it is assumed that Pillar II fails first and loses its bearing capacity suddenly, and then the bearing load of Pillar II will transfer to pillars I and III due to the elastic rebound of disc spring group. The failure process is analyzed as follows:

When the stress of Pillar II reaches peak strength, the deformation of near-field surrounding rockmass and treble-pillar specimen are D_1 and d_1, respectively. Then, the load F_1 at this critical moment can be expressed as follows:

$$F_1 = \left(k_{\mathrm{I}} + k_{\mathrm{II}} + k_{\mathrm{III}}\right)d_1 = KD_1. \tag{1}$$

After Pillar II fails, the deformation of near-field surrounding rockmass rebounds to D_2; while the deformation of treble-pillar specimen increases to d_2. The load F_2 can be expressed as follows:

$$F_2 = \left(k_{\mathrm{I}} + k_{\mathrm{III}}\right)d_2 = KD_2. \tag{2}$$

As a result, the load drop ΔF and sudden jump Δd of pillars-surrounding rockmass system can be expressed as follows:

$$\begin{cases} \Delta F = F_1 - F_2 \\ \Delta d = D_1 - D_2 = d_2 - d_1 \end{cases}. \tag{3}$$

The total displacement D_{T} of the pillars-surrounding rockmass system remains constant after Pillar II fails, as shown in Fig. 10a and Eq. (4):

$$D_{\mathrm{T}} = D_1 + d_1 = D_2 + d_2. \tag{4}$$

By combining the Eqs. (1) ~ (3), it is calculated that

$$\begin{cases} \Delta d = \frac{k_{\mathrm{II}} d_1}{k_{\mathrm{I}} + k_{\mathrm{III}} + K} \\ \Delta F_{\mathrm{I}} = k_{\mathrm{I}} \Delta d \\ \Delta F_{\mathrm{III}} = k_{\mathrm{III}} \Delta d \\ \Delta F = K \Delta d \end{cases}, \tag{5}$$

where ΔF_{I} and ΔF_{III} are the transferred load from Pillar II to pillars I and III, respectively.

More generally, when two or more pillars fail simultaneously in the parallel pillars ($n \geq 3$), the following equations can be obtained:

$$\begin{cases} \Delta d = \frac{d_1 \sum k_{\mathrm{d}}}{\sum k_{\mathrm{ud}} + K} \\ \Delta F_i = k_i \Delta d \\ \Delta F = K \Delta d \end{cases}, \tag{6}$$

where Σk_{d} is the sum of pre-peak stiffness of all the damaged pillars; Σk_{ud} is the sum of pre-peak stiffness of all the undamaged intact pillars; ΔF_i is the transferred load from damaged pillars to the undamaged pillar i; k_i is the pre-peak stiffness of undamaged pillar i.

When the stiffness of near-field surrounding rockmass (K) tends to infinity, which means the stiff loading condition in Fig. 10b, the failure of Pillar II will not cause sudden jump Δd. As a result, the failure of Pillar II will not cause the load transfer in pillars I and III; and the load drop ΔF equals the load drop of Pillar II (which is $k_{\mathrm{II}} d_1$).

Based on the above theoretical analysis, the theoretical values of sudden jump displacement and load transfer of treble-pillar specimen were calculated and compared with the experimental results, as shown in Fig. 11. In this respect, the

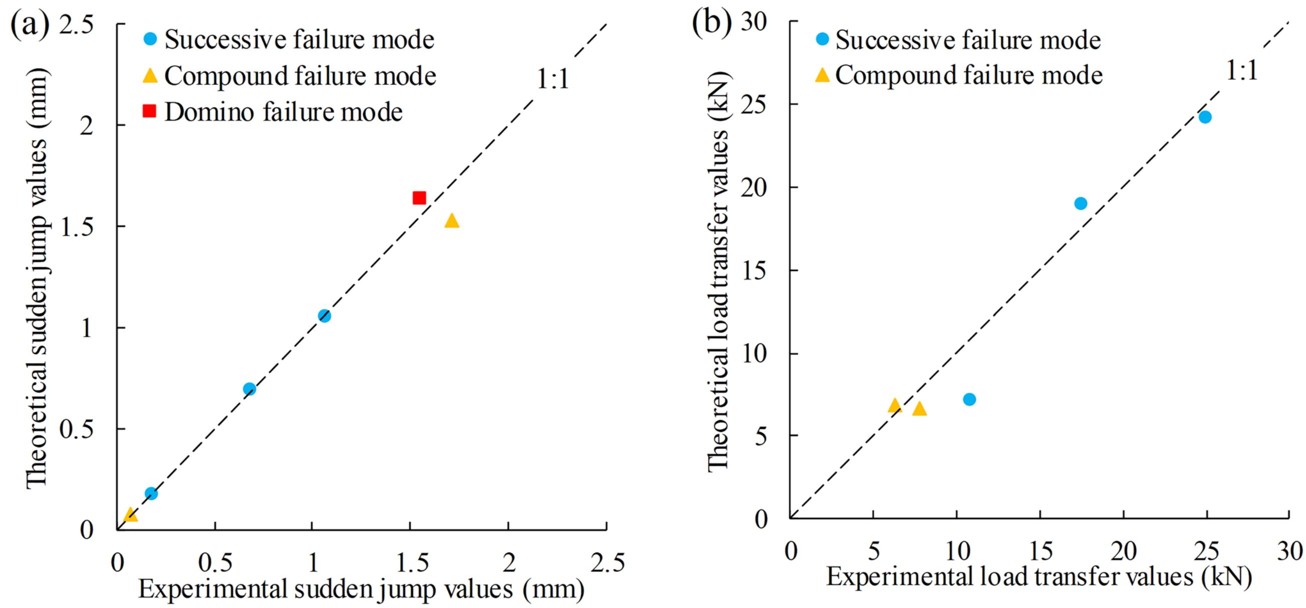

Fig. 11 The comparison between experimental values and theoretical values. **a** Sudden jump values (Δd) of treble-pillar specimen; **b** load transfer values (ΔF_i) of treble-pillar specimen

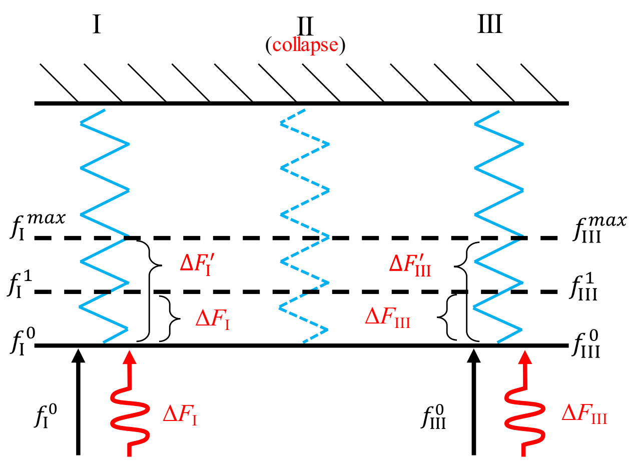

Fig. 12 Dynamic response of pre-stressed pillars subjected to a suddenly applied loading

theoretical values were in good agreement with the experimental results.

Additionally, the dynamic load should be considered by introducing the dynamic amplification factor ($R_{\mathrm{I}}^{\max}$ and $R_{\mathrm{III}}^{\max}$) in order to reproduce the real pillar failure mechanism. As shown in Fig. 12, after Pillar II collapses, the load previously carried by it will be redistributed and act on neighboring pillars (I and III). The transferred load can be given as follows:

$$\begin{cases} \Delta F_{\mathrm{I}} = f_{\mathrm{I}}^{1} - f_{\mathrm{I}}^{0} \\ \Delta F_{\mathrm{III}} = f_{\mathrm{III}}^{1} - f_{\mathrm{III}}^{0} \end{cases}, \tag{7}$$

where f_{I}^{0} and f_{III}^{0} are pillar stresses before Pillar II collapses, and f_{I}^{1} and f_{III}^{1} are pillar stresses after Pillar II collapses. And they are given by the following:

$$\begin{cases} f_{\mathrm{I}}^{0} = k_{\mathrm{I}} d_1 \\ f_{\mathrm{III}}^{0} = k_{\mathrm{III}} d_1 \\ f_{\mathrm{I}}^{1} = k_{\mathrm{I}} d_2 \\ f_{\mathrm{III}}^{1} = k_{\mathrm{III}} d_2 \end{cases}. \tag{8}$$

Figure 12 illustrates the dynamic response of pre-stressed pillars (I and III) subjected to a suddenly applied load induced by Pillar II collapses. The pillars (I and III) are initially under compressive stresses f_{I}^{0} and f_{III}^{0}. When the transferred load is applied, the stress equilibrium is disturbed, and the pillar compression undergoes an acceleration stage until the vertical loads of pillars (I and III) reach f_{I}^{1} and f_{III}^{1}. At that moment, the pillar loads are equal to the external load, indicating that it would be the equilibrium position for the pillars. Then, the speed of pillar compression declines until reaching the maximum compressional position. The pillars would oscillate around and finally converge to the equilibrium position.

The induced disturbance to pillars (I and III) can be characterized by the dynamic amplification coefficient R, defined as the ratio of the dynamic increased load to the final transferred load. The maximum dynamic amplification coefficient is achieved at the maximum compressive position. The maximum loads ($f_{\mathrm{I}}^{\max}$ and $f_{\mathrm{III}}^{\max}$) of Pillar I and Pillar III can be expressed in terms of $R_{\mathrm{I}}^{\max}$ and $R_{\mathrm{III}}^{\max}$ respectively:

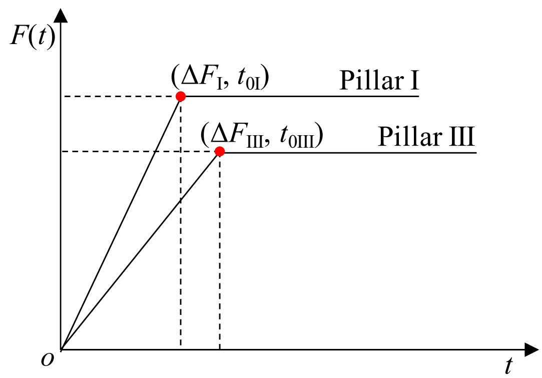

Fig. 13 Loading history of transferred loads to Pillar I and Pillar III

$$\begin{cases} f_{\mathrm{I}}^{\max} = f_{\mathrm{I}}^{0} + \Delta F_{I}^{'} = f_{\mathrm{I}}^{0} + R_{\mathrm{I}}^{\max}\Delta F_{\mathrm{I}} \\ f_{\mathrm{III}}^{\max} = f_{\mathrm{III}}^{0} + \Delta F_{III}^{'} = f_{\mathrm{III}}^{0} + R_{\mathrm{III}}^{\max}\Delta F_{\mathrm{III}} \end{cases}. \tag{9}$$

When Pillar II collapses, the support to the roof is released in a very short time, and the overburden loads are transferred to Pillar I and Pillar III. The load transfer duration is assumed as $t_{0\mathrm{I}}$ and $t_{0\mathrm{III}}$. Since Pillar I and Pillar III deform simultaneously, $t_{0\mathrm{I}}$ is considered to be equal to $t_{0\mathrm{III}}$. For adjacent pillars, the time-dependent transferred load is considered as a single ramp loading followed by constant loading, as illustrated in Fig. 13. Thus, the loading history of Pillar I and Pillar III can be mathematically expressed as:

$$F(t) = \begin{cases} \frac{\Delta F_{\mathrm{I}}}{t_{0\mathrm{I}}} t\left(t < t_{0\mathrm{I}}\right) \\ \Delta F_{\mathrm{I}}\left(t \geq t_{0\mathrm{I}}\right) \\ \frac{\Delta F_{\mathrm{III}}}{t_{0\mathrm{III}}} t\left(t < t_{0\mathrm{III}}\right) \\ \Delta F_{\mathrm{III}}\left(t \geq t_{0\mathrm{III}}\right) \end{cases}. \tag{10}$$

According to the dynamic load $F(t)$, the maximum dynamic amplification coefficients $R_{\mathrm{I}}^{\max}$ and $R_{\mathrm{III}}^{\max}$ of Pillar I and Pillar III can be obtained using the method of Zhou et al. (2018b):

$$\begin{cases} R_{\mathrm{I}}^{\max} = max\left[\begin{array}{c} \frac{1}{t_{0\mathrm{I}}}\left(t - \frac{T_{\mathrm{I}}}{2\pi}\sin\frac{2\pi}{T_{\mathrm{I}}}t\right)\left(t < t_{0\mathrm{I}}\right) \\ 1 - \frac{T_{\mathrm{I}}}{\pi t_{0\mathrm{I}}}\cos\frac{2\pi}{T_{\mathrm{I}}}\left(t - \frac{t_{0\mathrm{I}}}{2}\right)\sin\frac{\pi t_{0\mathrm{I}}}{T_{\mathrm{I}}}\left(t \geq t_{0\mathrm{I}}\right) \end{array}\right] \\ R_{\mathrm{III}}^{\max} = max\left[\begin{array}{c} \frac{1}{t_{0\mathrm{III}}}\left(t - \frac{T_{\mathrm{III}}}{2\pi}\sin\frac{2\pi}{T_{\mathrm{III}}}t\right)\left(t < t_{0\mathrm{III}}\right) \\ 1 - \frac{T_{\mathrm{III}}}{\pi t_{0\mathrm{III}}}\cos\frac{2\pi}{T_{\mathrm{III}}}\left(t - \frac{t_{0\mathrm{III}}}{2}\right)\sin\frac{\pi t_{0\mathrm{III}}}{T_{\mathrm{III}}}\left(t \geq t_{0\mathrm{III}}\right) \end{array}\right] \end{cases}, \tag{11}$$

where T_{I} and T_{III} are the natural vibration period of Pillar I and Pillar III, respectively.

5 Conclusions

In this study, the load transfer behavior of treble-pillar specimen was investigated based on laboratory tests. The effect of elastic rebound of near-field surrounding rockmass on the failure behavior of treble-pillar specimen was investigated, which revealed the physical essence of load and energy transfer. The following conclusions can be drawn:

(1) The elastic deformation of near-field surrounding rockmass (or the soft loading condition) is the necessary condition for the load transfer of multiple pillars; and the rapid elastic rebound of near-field surrounding rockmass is the physical essence that induces the load transfer behavior. The experimental results showed no load transfer when the treble-pillar specimen was under stiff loading condition due to the lack of elastic rebound of near-field surrounding rockmass.

(2) The failure behavior of different combination modes of treble-pillar specimen under soft loading condition can be summarized into three failure modes, which are successive failure mode, compound failure mode and domino failure mode. The successive failure mode needs the continued external loading to complete the failure of all three pillars of treble-pillar specimen; the domino failure mode can spontaneously complete the failure of all three pillars relying on the elastic rebound of near-field surrounding rockmass without the need of continued external loading from test machine; and the compound failure mode is a transition mode between them both including the continued external loading and elastic rebound.

(3) The proposed theoretical model further clarified the mechanism of load transfer behavior of parallel pillars under soft loading condition. The load transfer and the sudden jump displacement of treble-pillar specimen were estimated by using the theoretical model, where the theoretical results were in good agreement with the experimental results. This study contributes to the better understanding of load transfer mechanism of many parallel pillars in underground mining engineering.

(4) In underground engineering, it is very important to quickly and accurately find the weakest pillar and further determine the failure sequence of pillars. In this respect, the stress concentration and transfer among pillars are still the basis problem, which may be monitored and analyzed based on equations proposed in this study. In future study, we should focus on the prediction of failure sequence of pillars, as well as the effects of initial damage (such as joints and fractures) on the load transfer behavior and unstable failure mode of multi-

pillar specimen, in order to effectively predict the cascading pillar failure in underground mines.

Acknowledgements This work is funded by the National Natural Science Foundation of China (Grant nos. U1906208, 51874069 and 51904057), Liaoning Revitalization Talents Program of China (no. XLYC1802031) and the Fundamental Research Funds for the Central Universities of China (Grant nos. N2101015 and N180106003).

References

Chen ZH, Tang CA, Huang RQ (1997) A double rock sample model for rockbursts. Int J Rock Mech Min Sci 34:991–1000. https://doi.org/10.1016/S1365-1609(97)80008-1

Chen ZH, Gan Y, Labuz JF (2008) Analytical and numerical study of the size effect on the failure response of hierarchical structures. Int J Multiscale Comput Eng 6:339–348. https://doi.org/10.1615/IntJMultCompEng.v6.i4.50

Cording EJ, Hashash YMA, Oh J (2015) Analysis of pillar stability of mined gas storage caverns in shale formations. Eng Geol 184:71–80. https://doi.org/10.1016/j.enggeo.2014.11.001

Dehghan S, Shahriar K, Maarefvand P et al (2013) 3-D numerical modelling of Domino failure of hard rock pillars in Fetr6 Chromite Mine, Iran, and comparison with empirical methods. J Cent South Univ 20:541–549. https://doi.org/10.1007/s11771-013-1517-8

Esterhuizen GS, Tyrna PL, Murphy MM (2019) A case study of the collapse of slender pillars affected by through-going discontinuities at a limestone mine in Pennsylvania. Rock Mech Rock Eng 52:4941–4952. https://doi.org/10.1007/s00603-019-01959-6

Gao F, Kang H, Lou J et al (2019) Evolution of local mine stiffness with mining process: insight from physical and numerical modeling. Rock Mech Rock Eng 52:3947–3958. https://doi.org/10.1007/s00603-019-01798-5

Kaiser PK, Tang CA (1998) Numerical simulation of damage accumulation and seismic energy release during brittle rock failure-part II: rib pillar collapse. Int J Rock Mech Min Sci 35:123–134. https://doi.org/10.1016/S0148-9062(97)00010-7

Labuz JF, Biolzi L (1991) Class I vs Class II stability: a demonstration of size effect. Int J Rock Mech Min Sci Geomech Abstr 28:199–205. https://doi.org/10.1016/0148-9062(91)92167-W

Ma T-H, Tang C-A, Tang S-B et al (2018) Rockburst mechanism and prediction based on microseismic monitoring. Int J Rock Mech Min Sci 110:177–188. https://doi.org/10.1016/j.ijrmms.2018.07.016

Peng SS (2007) Ground control failures—a pictorial view of case studies. West Virginia University Press, Morgantown

Salamon MDG (1970) Stability, instability and design of pillar workings. Int J Rock Mech Min Sci Geomech Abstr 7:613–631. https://doi.org/10.1016/0148-9062(70)90022-7

Shannon CE (1948) A mathematical theory of communication. Bell Syst Tech J 27:623–656. https://doi.org/10.1002/j.1538-7305.1948.tb01338.x

Swanson PL, Boler FM (1995) The magnitude 5.3 seismic event and collapse of the solvay trona mine: analysis of pillar/floor failure stability. United States Bureau of Mines open fire report

Szwedzicki T (2001) Geotechnical precursors to large-scale ground collapse in mines. Int J Rock Mech Min Sci 38:957–965. https://doi.org/10.1016/S1365-1609(01)00062-4

Vardar O, Tahmasebinia F, Zhang C et al (2017) A review of uncontrolled pillar failures. Procedia Eng 191:631–637. https://doi.org/10.1016/j.proeng.2017.05.227

Wang JA, Shang XC, Ma HT (2008) Investigation of catastrophic ground collapse in Xingtai gypsum mines in China. Int J Rock Mech Min Sci 45:1480–1499. https://doi.org/10.1016/j.ijrmms.2008.02.012

Wang SY, Sloan SW, Huang ML et al (2011) Numerical study of failure mechanism of serial and parallel rock pillars. Rock Mech Rock Eng 44:179–198. https://doi.org/10.1007/s00603-010-0116-3

Xia K, Chen C, Zhou Y et al (2019) Catastrophe instability mechanism of the pillar-roof system in gypsum mines due to the influence of relative humidity. Int J Geomech 19:1–16. https://doi.org/10.1061/(ASCE)GM.1943-5622.0001378

Zhang J, Huang P, Zhang Q et al (2017) Stability and control of room mining coal pillars-taking room mining coal pillars of solid backfill recovery as an example. J Cent South Univ 24:1121–1132. https://doi.org/10.1007/s11771-017-3515-8

Zhou Z, Chen L, Zhao Y et al (2017) Experimental and numerical investigation on the bearing and failure mechanism of multiple pillars under overburden. Rock Mech Rock Eng 50:995–1010. https://doi.org/10.1007/s00603-016-1140-8

Zhou Z, Chen L, Cai X et al (2018a) Experimental investigation of the progressive failure of multiple pillar-roof system. Rock Mech Rock Eng 51:1629–1636. https://doi.org/10.1007/s00603-018-1441-1

Zhou Z, Zhao Y, Cao W et al (2018b) Dynamic response of pillar workings induced by sudden pillar recovery. Rock Mech Rock Eng 51:3075–3090. https://doi.org/10.1007/s00603-018-1505-2

Zhou Z, Zang H, Cao W et al (2019) Risk assessment for the cascading failure of underground pillar sections considering interaction between pillars. Int J Rock Mech Min Sci 124:104142. https://doi.org/10.1016/j.ijrmms.2019.104142

Zhou Z, Wang H, Cai X et al (2020) Bearing characteristics and fatigue damage mechanism of multi-pillar system subjected to different cyclic loads. J Cent South Univ 2:542–553. https://doi.org/10.1007/s11771-020-4315-0

Zhu W, Chen L, Zhou Z et al (2018) Failure propagation of pillars and roof in a room and pillar mine induced by Longwall mining in the lower seam. Rock Mech Rock Eng. https://doi.org/10.1007/s00603-018-1630-y

Zhu D, Song X, Li H et al (2020) Cooperative load-bearing characteristics of a pillar group and a gob pile in partially caved areas at shallow depth. Energy Sci Eng 8:89–103. https://doi.org/10.1002/ese3.511

Zipf RK (1996) Simulation of cascading pillar failure in room-and-pillar mines using boundary-element-method. Paper presented at the 2nd North American Rock Mechanics Symposium, Montreal, Quebec, Canada, 1996/1/1/

Zipf RK (2011) Toward pillar design to prevent collapse of room and pillar mines. NIOSH-Spokane Research Laboratory, Spokane

Zipf RK, Mark C (1997) Design methods to control violent pillar failures in room-and-pillar mines. Min Technol IMM Trans Sect A 106:A124–A132